3D Printing in Medicine

RESEARCH

Open Access

Biomechanical design considerations of a 3D-printed tibiotalocalcaneal nail for ankle joint fusion

Kin Weng Wong[1,2], Shao-Fu Huang[3,4], Skye Hsin-Hsien Yeh[5,6], Tai-Hua Yang[1,7,8], Cheng-Yi Liang[9] and Chun-Li Lin[3,4*]

Abstract

Tibiotalocalcaneal (TTC) arthrodesis treatment using intramedullary nails faces significant challenges due to inadequate bone integration and mechanical stability. This study developed a novel 3D-printed long titanium TTC intramedullary nail incorporating diamond lattice structures and differential thread leads to enhance biological fixation and compression. Four 3D-printed TTC nails (5 mm diameter, 70 mm length) with solid (TTC 1), lattice structure (TTC 2), lattice with longitudinal ribs (TTC 3), and lattice with both longitudinal and transverse ribs (TTC 4) were designed and manufactured. The lattice region featured a diamond array (70% porosity, 650 µm pore size, 1.2 mm unit length) with 2.5 mm thickness surrounding a 2.5 mm solid core. Static four-point bending tests assessed mechanical strength following ASTM F1264 protocols. Six skeletally mature Yorkshire pigs underwent TTC arthrodesis using TTC 1, 2, and 4 designs. Outcomes were evaluated using radiographic imaging and micro-CT analysis at 12 weeks post-surgery. All 3D-printed nails demonstrated acceptable precision with errors below 5% for straightness, circularity, and pitch distance. Mechanical testing revealed fracture strengths of 2387.33 ± 32.88 N, 435.00 ± 50.00 N, 849.17 ± 63.98 N, and 1133.67 ± 81.28 N for TTC 1–4, respectively. The differential thread design achieved significant compression ratios (81-82.5%) at fusion sites. Micro-CT analysis showed significantly higher bone formation in lattice designs (TTC 2: 145.37 ± 37.35 mm^3, TTC 4: 137.81 ± 9.52 mm^3) compared to the solid design (TTC 1: 28.085 ± 3.21 mm^3). However, TTC 2 experienced two implant fractures, while TTC 4 maintained structural integrity while promoting substantial bone growth. This study concluded that titanium 3D printing technology can be applied for manufacturing long TTC intramedullary nails with surface lattice design but reinforcing ribs need to be added to provide enough mechanical strength.

Keywords Tibiotalocalcaneal arthrodesis, 3D printing, Intramedullary nail, Lattice, Four-point bending

*Correspondence:
Chun-Li Lin
cllin2@nycu.edu.tw
[1]Department of Biomedical Engineering, College of Engineering, National Cheng Kung University, Tainan, Taiwan
[2]Department of Orthopedic Surgery, Chi Mei Medical Center, Tainan, Taiwan
[3]Department of Biomedical Engineering, National Yang Ming Chaio Tung University, Hsinchu, Taiwan
[4]Medical Device Innovation & Translation Center, National Yang Ming Chiao Tung University, 112, No.155, Sec.2, Linong Street, Taipei, Taiwan
[5]School of Medicine, National Defense Medical Center, Taipei, Taiwan
[6]Brain Research Center, National Yang Ming Chiao Tung University, Taipei, Taiwan
[7]Department of Orthopedic Surgery, College of Medicine, National Cheng Kung University Hospital, National Cheng Kung University, Tainan, Taiwan
[8]Medical Device Innovation Center, National Cheng Kung University, Tainan, Taiwan
[9]Kang Chiao International School Xiugang Campus, New Taipei City, Taiwan

Introduction

Tibiotalocalcaneal (TTC) nail is a specialized orthopedic implant used in foot and ankle surgeries to provide pain-free, stable plantigrade feet [1–4]. It is used to span the calcaneus, the talus and the distal tibia in a retrograde manner, fusing the subtalar joint and the ankle joint (Fig. 1). This surgery is becoming increasingly common and can be used to treat severe ankle and/or subtalar joint arthritis, acute severe fractures around the ankle, Charcot neuroarthropathy, severe ankle/hindfoot deformity, failed total ankle replacement and failed previous arthrodesis [3–9].

The clinical literature shows that TTC arthrodesis success rates range from 70% to as high as 90%. However, in complex cases involving severe deformities, large bone defects, revision surgery, diabetes, Charcot arthropathy, or smoking, nonunion rates may be as high as 50% [1, 3, 10–12]. The TTC nail mechanical behavior after implantation is strongly related to the surgical success rate. Typically, the main causes of failure are TTC nail loosening and incomplete fusion between the joint fusion site and the nail-bone interface [13–15]. Current commercially available retrograde TTC nails usually feature a long cylindrical design with a smooth surface, a circular cross-section, and manufactured using CNC turning. This design lacks sufficient anti-rotation capability, which can lead to relative motion between the bone and the intramedullary nail, resulting in poor interface fixation (Fig. 1). Additionally, this may cause the lateral locking screws to bear more force to stabilize the system, potentially leading to breakage. The commercially available products design may also result in insufficient compressive force between the bone segments, leading to inadequate contact at the joint fusion site bone bed, and incomplete healing.

Titanium 3D printing technology has progressively matured over the years and is now widely applied in implant manufacturing. In addition to its ability to customize (patient-specific) implants to match the geometric requirements of bone defects, another important advantage of this technology is its capacity to create diverse microstructures, such as lattice pore structures [16, 17]. Many studies have focused on various lattice design parameters, including morphology, size, and porosity, and their effects on mechanical strength and cellular proliferation [18–20]. Current literature indicates that porous titanium alloy implants produced by 3D printing, with a porosity of 60–70% and pore sizes less than 800 μm, can generate biologically active and mechanically stable surfaces. Therefore, utilizing 3D-printed

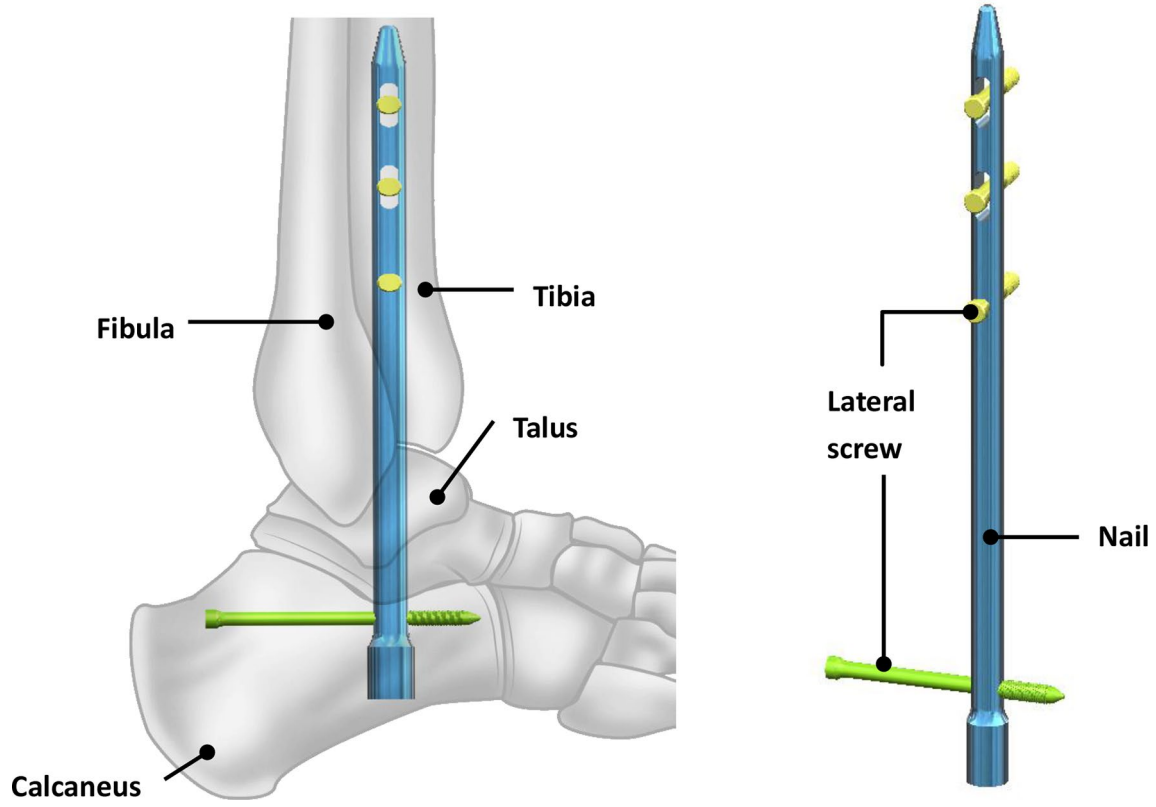

Fig. 1 Typical commercialized tibiotalocalcaneal (TTC) nail design. Standard intramedullary nail with circular cross-section, indicated for ankle and subtalar arthrodesis. Note the smooth surface and absence of compression features in this basic design

lattice manufacturing technology for TTC nails could facilitate effective bone cell integration with the implant [11, 21, 22]. However, incorporating the lattice structure while maintaining adequate mechanical strength presents a significant engineering challenge, particularly given the nail's cylindrical geometry and threaded structure. Additionally, manufacturing precision, specifically regarding cylindrical straightness and thread profile integrity, must be tightly controlled to ensure successful implantation.

This study utilizes titanium 3D printing technology to develop a novel TTC nail featuring a cylindrical geometry with threaded structure and surface lattice design. The manufacturing precision of the 3D-printed titanium TTC nail was validated using dimensional analysis, focusing on straightness, circularity, and thread specifications. The design incorporates various rib reinforcements to optimize mechanical strength, and multiple thread leads to enhance bone compression. Through in vivo pig experiments, this novel TTC nail design aims to demonstrate sufficient mechanical strength while promoting bone integration and improving surgical outcomes.

Materials and methods

3D printed TTC nail design and manufacture

A novel modified titanium TTC nail with 5 mm in diameter and 70 mm in length was designed to accommodate the pig bone size (Fig. 2). The nail's thread design incorporates two distinct leads, i.e. a distal single-start thread with a 3 mm pitch, and a proximal triple-start thread with a 9 mm pitch. This design allows the nail to advance axially by 3.0 mm and 9.0 mm respectively with each full rotation (360°) [23, 24]. The proximal and distal leads were positioned to correspond with the calcaneus and tibia, creating a compression effect between the double leads and significant compression over the fusion sites (Fig. 2).

Four different TTC nail designs, noted as TTC 1, 2, 3 and 4 were developed based on the previously described lead design (Fig. 3(a)). The TTC 1, serving as the baseline design, was a solid nail with 5 mm diameter. The TTC 2 featured a central solid core with 2.5 mm diameter surrounded by a region of three-dimensional lattice structures with 2.5 mm thickness and 25 mm in length from the proximal thread end was designed to enhance bone cell-seeding ability (Fig. 3(b)). This lattice scaffold incorporated a diamond structure array arrangement with 70% porosity, 650 μm pore sizes, 1.2 mm unit length, and 0.3 mm pillar diameter (Fig. 3(b)). The second TTC design added four longitudinal ribs of 1 mm thickness for improved mechanical strength. TTC 4 further enhanced structural integrity by incorporating four longitudinal ridges and one transverse ridge at the middle of the lattice region (Fig. 3(b)). These varying designs enable systematic comparison of mechanical properties and biological integration capabilities.

3D-printed TTC nail manufacturing and dimension validation

The TTC nails were manufactured using a titanium 3D printer (AB400, Renishaw, Gloucestershire, UK) with Ti6Al4V titanium alloy powder, which has an average grain size of 30 μm. The 3D printing process utilized a

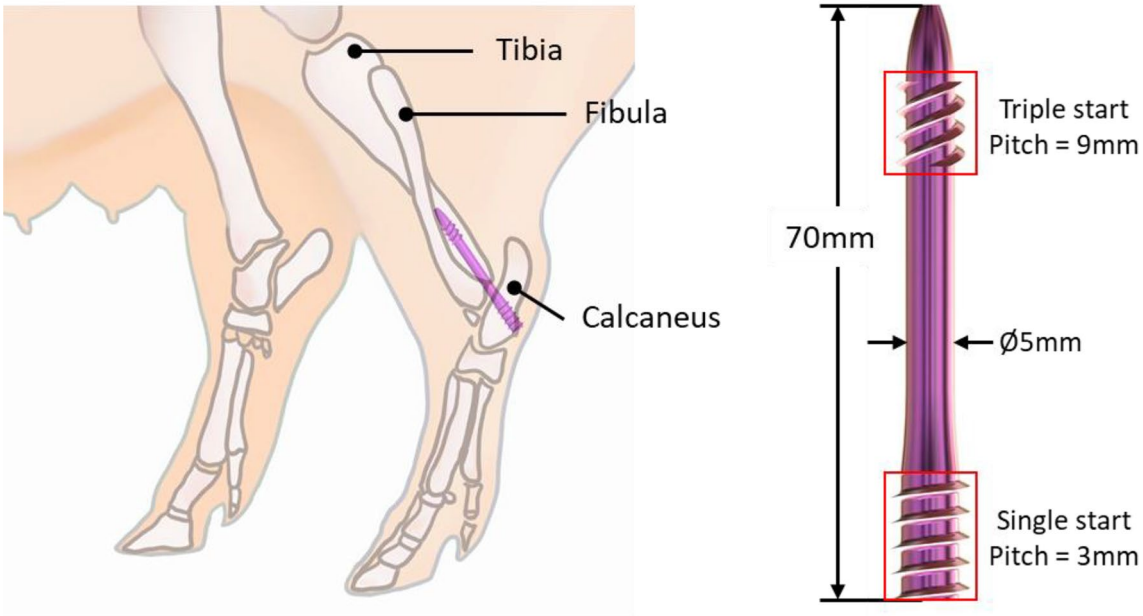

Fig. 2 Novel TTC nail design with dual-thread system for compression. The nail features a proximal single-start thread (3 mm pitch) and a distal triple-start thread (9 mm pitch), designed for retrograde insertion through the pig calcaneus, talus, and distal tibia

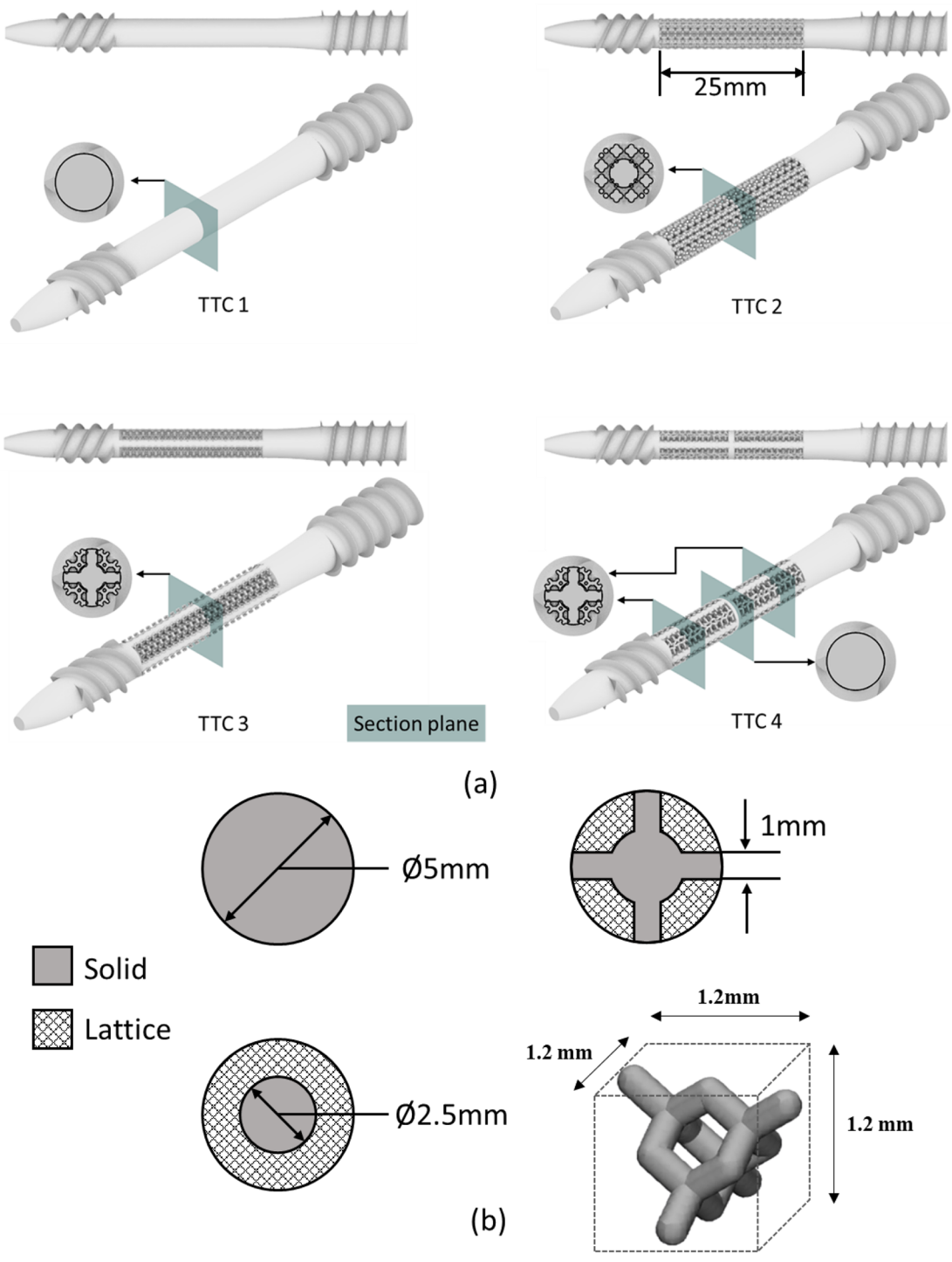

Fig. 3 Four TTC nail designs: (**a**) TTC 1: Baseline solid design (5 mm diameter), TTC 2: Core-lattice design (2.5 mm core, 25 mm lattice region), TTC 3: Core-lattice with longitudinal ribs and TTC 4: Core-lattice with longitudinal and transverse ribs; (**b**) Detailed specifications of the diamond array lattice structure: A 2.5 mm diameter central core with a 25 mm long lattice region featuring diamond-shaped patterns (70% porosity, 0.3 mm pillar diameter, 1.2 mm unit cells, 650 µm pore sizes). The lattice structure extends 2.5 mm from the central core, with additional 1 mm thick reinforcing ribs in TTC 3 and TTC 4 designs

laser power of 200 W, a scanning speed of 0.6 m/s, and an exposure time of 125 s. The laser selectively melted the powder, enabling it to crystallize and form the desired component. The manufacturing precision and layer thickness were consistently maintained at 30 µm. Afterward, the implants were cleaned once more using ultrasonic oscillations, as depicted in Fig. 4 (a).

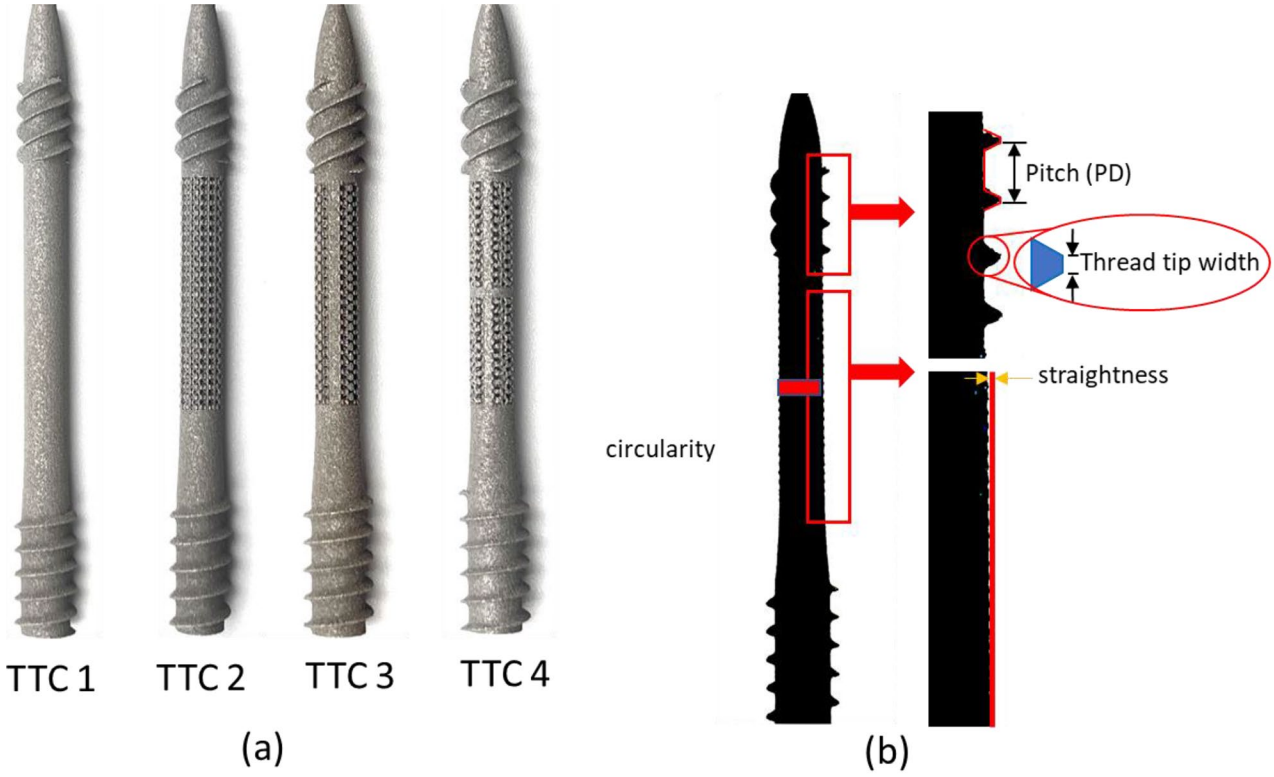

Fig. 4 (**a**) Four TTC nail designs (TTC1-4) manufactured using titanium 3D printing manufacturing. Final products after selective laser melting process, magnetic polishing, and ultrasonic cleaning. (**b**) Quality control measurements of the TTC nails demonstrating key dimensional parameters: circularity and straightness for insertion smoothness, thread pitch distance for accurate compression function, and thread tip width for optimal cutting performance

Since the object has a long cylindrical shape, the circularity (C) and straightness (S) errors must be minimal to permit nail to be inserted smoothly. The pitch distance (PD) of the thread must be accurate, and the cutting edge at the tip of the thread should be small to maintain cutting force (Fig. 4(b)). The dimensions designed in CAD as the actual dimensions and measured three samples of each of the four TTC types using a precision measuring system (ARCS Precision Technology Co., Ltd., Taiwan Region). The measured values were then compared with the corresponding actual values. We defined that the error for C, S and PD should be within 5%, and the thread tip width must be smaller than 0.2 mm, ensuring the printed accuracy of our TTC nail.

TTC nail biomechanical tests

Static four-point bending tests were conducted on the nails following American Society for Testing and Materials (ASTM) protocols (ASTM F1264) using an Instron E10000 testing machine (INSTRON, Canton, MA, USA) to provide comprehensive mechanical strength data. Static tests determined fracture strengths for the four nail designs. Nails were placed on a four-point bending test clamp with two rolling supports and loading rollers. A load was then applied at 3 mm/min until failure. The center span (a), span from load point to nearest support (b), and total span (L = a + 2b) were set at 17 mm, 17 mm, and 51 mm respectively, as per ASTM F1264 protocol (Fig. 5). Load-displacement diagrams were collected, and fracture strengths calculated at the intersection of the 0.2% offset line with the load-displacement curve. Failure patterns were visually examined to assess mechanisms. Based on these mechanical property test results, TTC 1, TTC 2, and TTC 4 were selected for the subsequent animal study. The decision to preclude TTC 3 from the animal study, despite its intermediate stiffness properties and elaborated upon in the discussion section.

In vivo pig experiment

The in vivo pig study was reviewed and approved by the Taiwan Instrument Research Institute (Protocol No.: NLAC-112-M-041-R2). All procedures were conducted in compliance with the ARRIVE (Animal research: reporting of in vivo experiments) guidelines, and all efforts were made to minimize the number of animals and amount of induced pain. Six skeletally mature Yorkshire pigs (2 male and 4 female), with an average age of nine months and weighing approximately 42 kg (Mean ± SD: 42.17 ± 0.24 kg), were used for this animal study. This pig model was selected due to its similarity

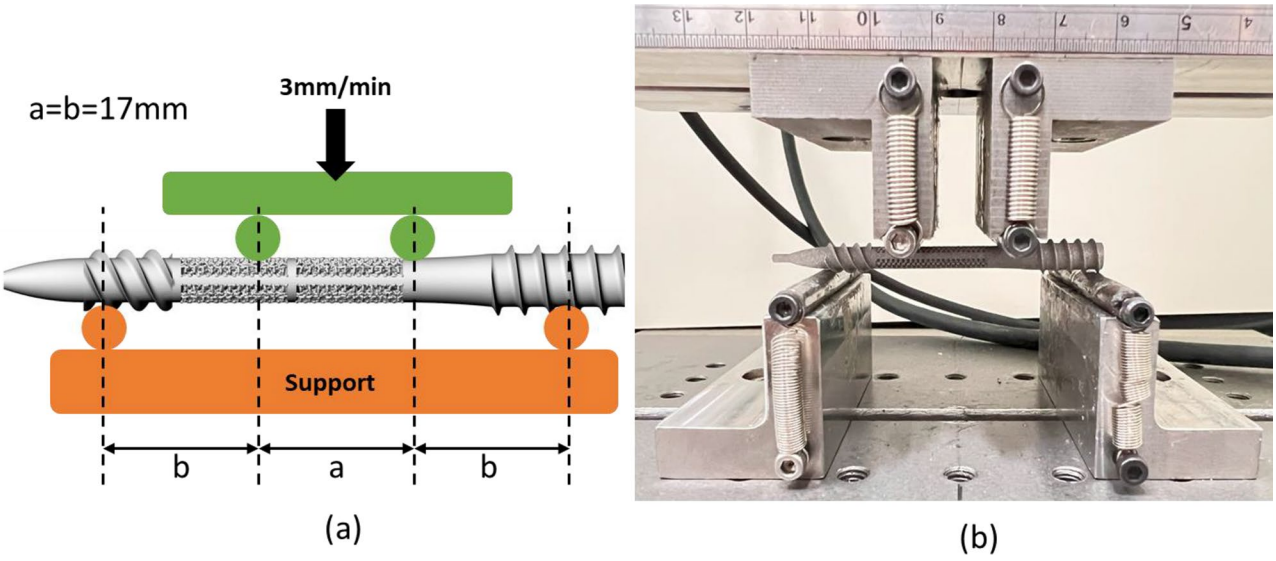

Fig. 5 Four-point bending test setup for TTC nails. (**a**) Schematic diagram illustrating standardized ASTM F1264 test configuration with critical measurements: center span (a = 17 mm), support span (b = 17 mm), and total span (L = 51 mm). (**b**) Actual test setup demonstrating four-point bending configuration physical implementation for mechanical strength evaluation

to the human bone structures in terms of bone quality, density, anatomy, and size. Additionally, pig offered lower variability among specimens and were more cost-effective for research purposes. Bone mineral density calculations were omitted from this study as all pigs were young and of similar age (9 months ± 1 week), minimizing age-related bone density variations that could impact the results.

In the animal study, the six pigs were distributed as follows: two pigs were assigned to test TTC 1 (solid nail), two for TTC 2 (porous lattice structure), and two for TTC 4 (porous lattice with longitudinal and transverse ribs). This distribution allowed for a comparison between the solid nail, the most porous design, and the design that balances porosity with enhanced mechanical properties.

The animals were fasted for a minimum of 12 h preoperatively, and anesthesia was administered according to the 'TIRI Y09 Standard Operating Procedure for Large Animal Anesthesia.' Pre-anesthetic medication was administered via intramuscular injection using a mixture of Telazol (2–5 mg/kg) and Xylazine (2.2 mg/kg). Following initial sedation, the surgical site was shaved, and the animal was weighed. Atropine (0.02–0.05 mg/kg) was administered subcutaneously to reduce excessive salivation and prevent aspiration pneumonia. For infection prophylaxis and pain management, Penicillin G (3–5 mL/animal) and either Meloxicam (0.4 mg/kg) or Buprenorphine (0.05–0.1 mg/kg) were administered intramuscularly. The animal was then transferred to the operating table, intubated, and maintained under general anesthesia using inhaled Isoflurane (0.2-6.0%) with an oxygen flow rate of 0.4–3.0 L/min. The vaporizer concentration was controlled via the gas anesthesia machine to achieve deep anesthesia.

Once sedated, the animal was positioned laterally, and the skin was thoroughly disinfected with Povidone-iodine. The surgeon then performed a lateral approach to the ankle, exposing both the ankle and subtalar joints. Meticulous debridement of the articular cartilage follows, preparing the joints for fusion. The optimal entry point on the plantar aspect of the calcaneus was identified. Under fluoroscopic guidance, a guide wire was carefully inserted, traversing the calcaneus and talus before entering the tibial medullary canal. This guide wire establishes the pathway for the nail. The guide wire canal was reamed to the appropriate diameter to accommodate the nail.

The TTC nail was carefully inserted and advanced through the prepared osseous pathway. During the nail insertion process, its unique compression mechanism was activated, providing optimal interfragmentary compression across the fusion sites (Fig. 6(a)). Following final fluoroscopic confirmation of proper hardware placement and alignment (Fig. 6(b)), the surgical site was thoroughly irrigated. Prior to closure, topical antibiotic (penicillin 3000 IU/kg; Penicillin G procaine, Ta Fong Pharmaceutical Co., Ltd., Changhua, Taiwan) was applied to control surgical site infection. The incision was then closed in layers. Post-operative care included appropriate pain management and activity restriction as per the study protocol. Surgical site CT images were taken immediately post-operative, and at the 4th and 12th weeks after surgery. At 12 weeks post-surgery, the pigs were euthanized under deep general anesthesia via heart exsanguination.

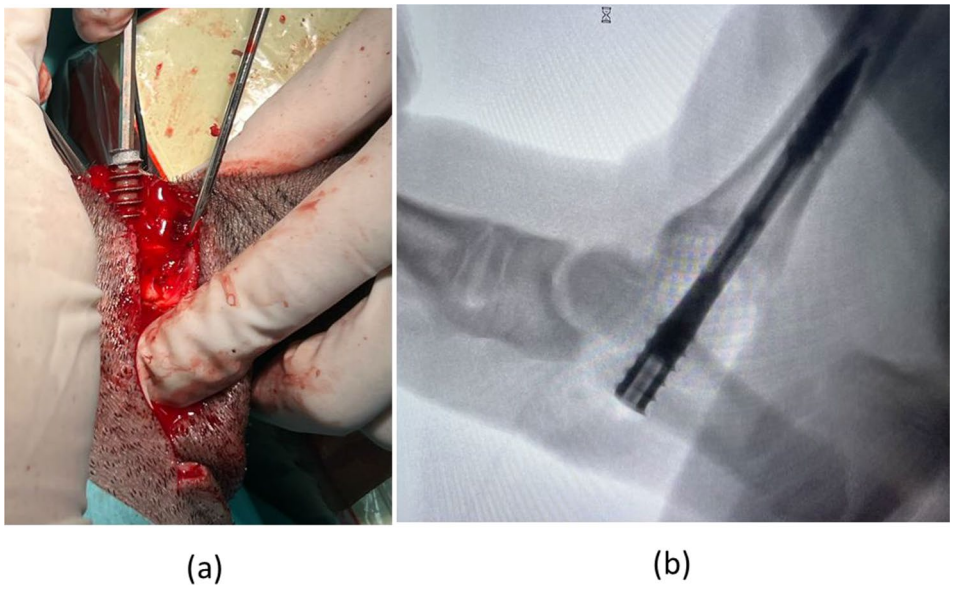

Fig. 6 TTC nail placement surgical procedure and imaging confirmation. (**a**) Intraoperative view of TTC nail insertion with compression mechanism activation; (**b**) Fluoroscopic confirmation showing final nail position and alignment

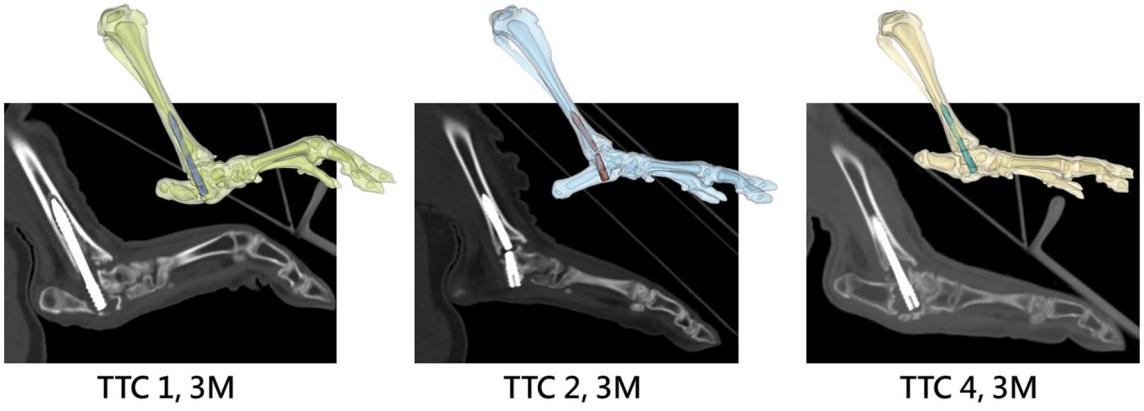

Fig. 7 Micro-CT analysis performed at postoperative 3 months showing trabecular bone structure around the implanted TTC 1, TTC 2 and TTC 4 nails, reconstructed at 5 μm resolution for detailed evaluation of bone integration. Note the fractured implant in TTC 2 group

The ankle joint was then removed and preserved in 4% formaldehyde solution for further analysis.

Micro CT image study

The removed bone and implant segments were examined using micro CT (micro-CT; MILabs, Utrecht, Netherlands) to analyze trabecular bone microarchitecture (Fig. 7). Imaging parameters included an X-ray voltage of 80 kVp, an anode current of 500 μA, and an exposure time of 300–350 milliseconds for each of the 360 rotational steps. These settings were optimized to achieve high-contrast bone tissue imaging while minimizing beam hardening artifacts. CT image reconstruction was performed using a Hann filter, achieving a voxel size of 5 μm.

To determine the volume of individual samples, regions of interest (ROIs) were delineated on each CT slice. The areas of the ROIs were summed across all slices, and the total was multiplied by the slice thickness to calculate sample volumes. The 3D volume renderings of the scan data were further processed using Imalytics Preclinical software (Gremse-IT GmbH, Germany). The detection area will be 27 mm in the middle of the implant (the porous lattice area), a virtual cylindrical ROI measuring 5.35 mm in diameter was generated for analysis.

To ensure consistency across all samples, the grayscale threshold for bone was standardized at 3500 Hounsfield units (HU) [25]. This standardization enabled quantitative assessment of the TTC nail volume within the defect site, facilitating comparisons of new bone formation among experimental groups.

Table 1 Quality control data for the TTC nail manufacturing precision

		Circularity	Straightness	Pitch	Thread tip (mm)
CAD	(mm)	5	0	3	0.05
TTC 1	#1	4.98	0.015	3.17	0.12
	#2	5.01	0.012	3.2	0.17
	#3	4.97	0.01	3.08	0.1
	Avg. ± std.	4.99 ± 0.2	0.012 ± 0.002	3.15 ± 0.05	0.13 ± 0.03
	error	-0.2%	1.20%	5.0%	N/A
TTC 2	#1	5.10	0.012	3.1	0.16
	#2	5.12	0.01	3.05	0.07
	#3	5.11	0.014	3.16	0.11
	Avg. ± std.	5.11 ± 0.01	0.012 ± 0.002	3.10 ± 0.04	0.11 ± 0.04
	error	2.2%	1.20%	3.4%	N/A
TTC 3	#1	5.14	0.011	3.08	0.06
	#2	5.10	0.013	3.06	0.16
	#3	5.12	0.01	3.14	0.13
	Avg. ± std.	5.12 ± 0.02	0.011 ± 0.001	3.09 ± 0.03	0.12 ± 0.04
	error	2.4%	1.10%	3.1%	N/A
TTC 4	#1	5.11	0.012	3.09	0.11
	#2	5.10	0.008	3.12	0.17
	#3	5.07	0.012	3.18	0.14
	Avg. ± std.	5.09 ± 0.02	0.011 ± 0.002	3.13 ± 0.04	0.14 ± 0.02
	error	1.8%	1.10%	4.3%	N/A

Results

The percentage calculation results for the manufacturing errors in C, S, and PD revealed that the largest error occurred in PD, reaching 4.3%. This was due to the helical characteristics of the thread. However, all errors were less than 5%, meeting the acceptance criteria. The maximum the thread tip width was only 0.17 mm, which demonstrated good precision for 3D-printed manufacturing. Not only does it meet the acceptance value of 0.2 mm, but it also maintained cutting functionality (Table 1).

The static four-point bending test results revealed varying fracture strength levels across the four TTC nail designs. TTC 1, the solid nail, demonstrated the highest fracture strength (2387.33 ± 32.88 N), serving as a baseline for comparison. TTC 4, featuring both longitudinal and transverse ribs, showed the second-highest fracture strength (1133.67 ± 81.28 N), followed by TTC 3 with longitudinal ribs (849.17 ± 63.98 N). TTC 2, designed with only porous lattice structure, exhibited the lowest fracture strength (435.00 ± 5.00 N) (Table 2).

For the animal study, two implant fractures were observed both in the TTC 2 group (porous lattice structure) during the follow-up periods (Fig. 8(a) and (b)). Despite these complications, all affected pigs maintained good overall health. After consultation with veterinary experts and in compliance with ARRIVE guidelines, it was determined that early termination of these pigs was not necessary. The study continued as planned for all subjects. Throughout the study, the body weights of all pigs were consistently monitored, with no significant variations observed. At the 12-week endpoint, no surgical wound infections or other complications were detected in any of the subjects. All animals were euthanized according to the predetermined schedule. Post-mortem X-ray imaging confirmed the earlier findings, showing that four out of six pigs maintained intact implants, while two exhibited the previously identified implant fractures.

To evaluate the TTC nail compression efficiency, the distance between the distal tibial articular end plate and the calcaneus subtalar articular end plate was measured in the sagittal plane using CT images obtained preoperatively and at 3 months postoperatively. The compression ratio was calculated as (postoperative distance/preoperative distance × 100%). Due to implant fractures, TTC 2 group data were excluded from this analysis. Results demonstrated effective compression capability in the remaining designs, with the TTC 4 group achieving an average compression ratio of 81%, comparable to the TTC 1 group at 82.5%. (Fig. 9; Table 2).

The micro-CT analysis revealed significant differences in implant volume and newly formed bone volume across the three TTC nail designs tested in this animal study. The implant volumes were as follows: TTC 1 (solid nail) had the highest volume at 528.21 mm^3, followed by TTC 4 (porous lattice with longitudinal and transverse ridges) at 435.55 mm^3, and TTC 2 (porous lattice structure) with the lowest volume at 393.78 mm^3 (Fig. 10).

The newly formed bone volume analysis revealed a trend that contrasted with the implant volume results. On average, TTC 2 (porous lattice structure) demonstrated the highest volume of newly formed bone (145.37 mm^3), followed closely by TTC 4 (longitudinal and transverse

Table 2 TTC nail design compressive capability ratio

		Implant condition	Pre-OP(mm)	Post OP(3 M)(mm)	Compression capability ratio (%)	Avg. (%)
TTC 1	#1	**Intact**	30.45	26.79	88	82.5
	#2	**Intact**	31.78	24.56	77	
TTC 4	#1	**Intact**	30.07	25.79	86	81.0
	#2	**Intact**	29.04	22.07	76	

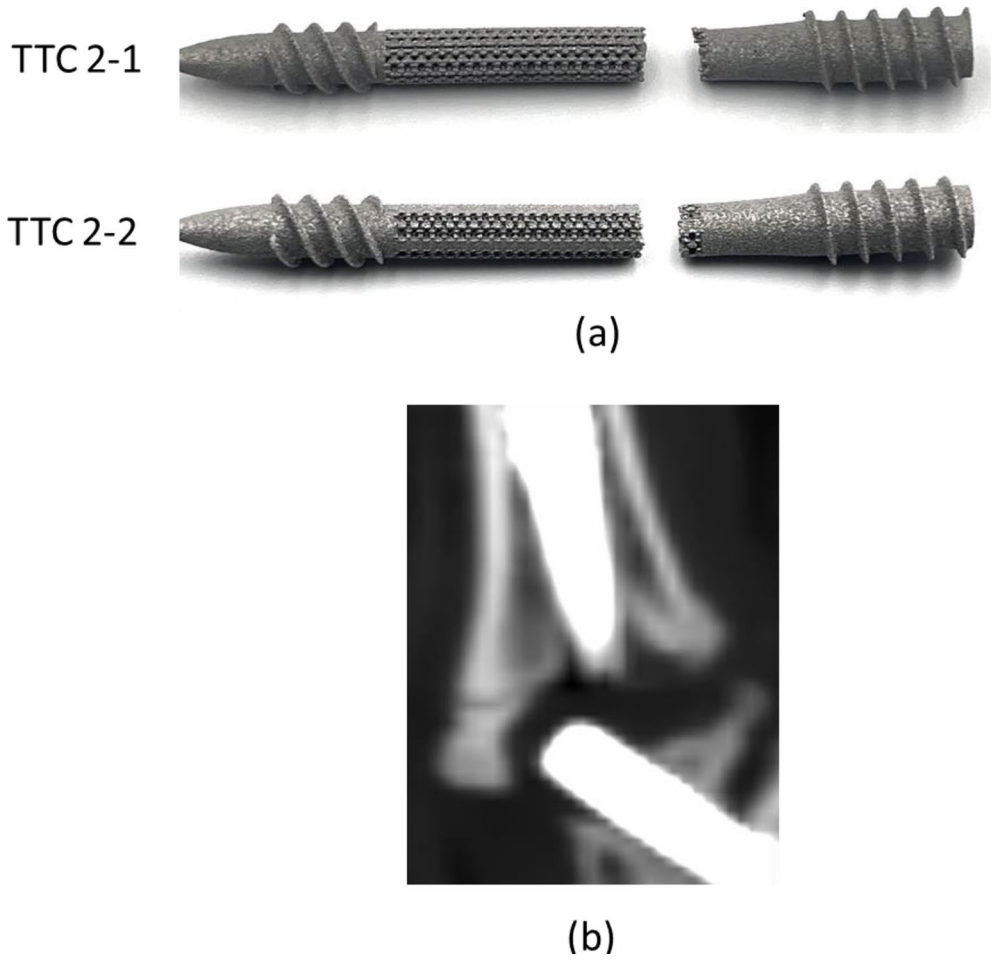

Fig. 8 (**a**) Schematic diagram showing fracture patterns in both TTC 2 nails; (**b**) Post-operative X-ray demonstrating fracture in a TTC 2 nail (porous lattice design). All subjects remained clinically stable throughout the study period

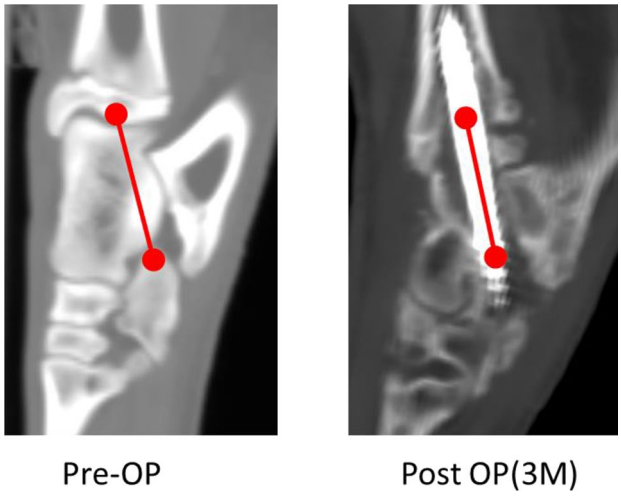

Fig. 9 Comparative analysis of the TTC nail compression effectiveness. CT measurements at sagittal plane showing bone distance between calcaneus and tibia before and 3 months after surgery. Compression capability ratio (postoperative/preoperative distance percentage) demonstrated superior performance of both TTC 1 and TTC 4 (82.5% and 81.0% compression rate respectively)

ridges) with 137.81 mm^3. In contrast, TTC 1 (solid nail), despite having the largest implant volume, showed the least new bone formation with only 28.085 mm^3. However, a closer examination of the individual results provides additional insights. Both pigs in the TTC 2 group experienced implant fractures, with newly formed bone volumes of 161.67 mm^3 and 108.85 mm^3 respectively (Table 3).

Discussion

This study used titanium 3D printing technology to manufacture the TTC nail, with the primary consideration being its excellent manufacturing capability for micro-lattices. This feature allowed the nail to promote bone growth, thereby enhancing stability after implantation. During the design phase, we also considered the need to improve the compression effect on the joint surface, which led to the design of two different thread pitches to strengthen the compression effect after implantation. However, since the TTC nail was an intramedullary nail with a length many times greater than its diameter,

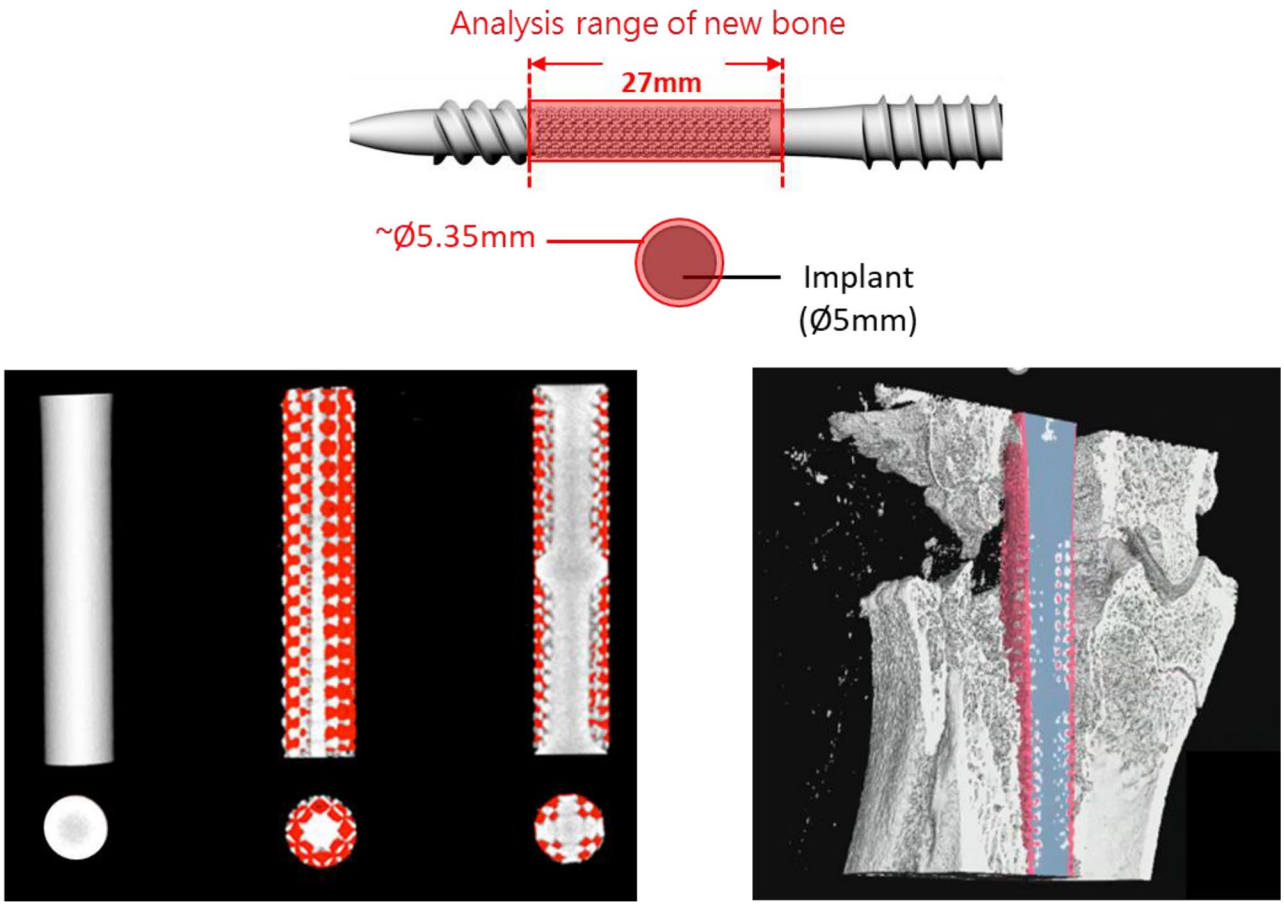

Fig. 10 Micro-CT analysis of newly formed bone formation around the TTC nails. The analysis ranges 27 mm in length and 5.35 mm in diameter covering the whole lattice region. The sagittal, the axial, and the 3D views: minimal bone growth on TT1 (solid nail); extensive bone integration (red) in porous TTC 2 and TTC 4, demonstrating their superior osteointegration performance

Table 3 Implant condition, implant volume, newly formed bone volume and static four-point bending test results for the TTC nail designs

No.	Implant condition	Implant volume (mm^3)	New bone volume (mm^3)	New bone volume avg. (mm^3)	Four-point bending fracture strength (*N*)
TTC 1 #1	**Intact**	528.21	38.06	28.085	2387.33 ± 32.88 N
TTC 1 #2	**Intact**		18.11		
TTC 2 #1	**Fracture**	393.78	161.67	145.37	435.00 ± 50.00 N
TTC 2#2	**Fracture**		108.85		
TTC 3 #1	N/A	410.48	N/A	N/A	849.17 ± 63.98 N
TTC 3 #2	N/A		N/A	N/A	
TTC 4 #1	**Intact**	435.55	144.54	137.81	1133.67 ± 81.28 N
TTC 4 #2	**Intact**		131.07		

attention was first given to ensuring the straightness of the final product. The results showed that straightness (S), circularity (C), and pitch diameter (PD) all fell within the acceptable error range. Additionally, the thread tip width was less than 0.2 mm, which is very close to the tip width of a traditional bone screw used for fixation with a 5 mm diameter screw (average width was 0.2 mm). This small deviation is an acceptable machining tolerance and allows for the cutting effect when the nail locks into place. The compression function design with different pitches showed that the nail was able to achieve compression that exceeded half of the preoperative joint gap distance, which aligns with clinical needs [21].

Furthermore, when designing the nail surface lattice structure, a balance had to be found between the nail's strength and its functionality. The static four-point

bending test results clearly demonstrated the significant impact of ribs designed on the nails' structural properties. The solid nail (TTC 1) exhibited the highest fracture strength at 2387.33 ± 32.88 N, serving as the benchmark. To address the low fracture strength of the initial porous design (TTC 2, 435.00 ± 50.00 N), structural modifications were incrementally implemented. The addition of four longitudinal ribs in TTC 3 nearly doubled the fracture strength to 849.17 ± 63.98 N compared to TTC 2. Further enhancement was achieved in TTC 4, where the combination of four longitudinal and one transverse rib tripled the fracture strength to 1133.67 ± 81.28 N relative to TTC 2. Notably, TTC 4 achieved approximately half the fracture strength of the solid nail (TTC 1), demonstrating an effective balance between structural integrity and the benefits of the porous lattice structure. These results highlight the effectiveness of the rib design in enhancing the porous nail mechanical properties while maintaining its potential biological advantages. This optimal balance achieved in TTC 4, coupled with the need to compare it against both the solid nail (TTC 1) and the purely porous design (TTC 2), informed the decision to focus on these three designs (TTC 1, TTC 2, and TTC 4) for the subsequent animal study. The intermediate design (TTC 3) was excluded as TTC 4 represented a more advanced iteration with superior mechanical properties.

Based on our knowledge, this study is the first to use pigs for ankle joint fusion surgery with novel 3D-printed TTC nails. There are several surgical techniques that require careful attention during the procedure. A crucial anatomical difference between pigs and humans that impacts surgical approach. Unlike in humans, the centers of the tibia, talus, and calcaneus in pigs do not align in a straight line in both sagittal and coronal planes. Consequently, if the implant's entry point in the calcaneus is too medially and posteriorly during surgery, it can lead to postoperative fractures. This complication underscores the critical importance of precise surgical technique, particularly in selecting the appropriate implant entry point and overall implant path. Optimal positioning is essential for the implant to securely anchor the surgical fusion area while avoiding local stress concentrations on both the implant and surrounding bone. This experience emphasizes the need for careful consideration of species-specific anatomy in animal models and the potential for adapting surgical techniques to account for these differences in future studies or clinical applications. For the two nails that fractured in the TTC 2 group, we believed the fractures occurred because their mechanical strength had already decreased to a quarter of the original strength, and they were unrelated to the surgical procedure.

This study used Micro-CT imaging to assess bone growth volume and morphology after TTC nails implantation. 3D Micro-CT provided information not obtainable through traditional 2D analysis. As an advanced, non-destructive technology, it offered high resolution, wide sample adaptability, and detailed visualization of complex microarchitectures, making it an effective tool for analyzing porous metallic implants [6, 26, 27]. Studies also confirmed a strong correlation between quantitative histomorphometry and 3D Micro-CT measurements, especially for bone area/volume in and around porous structures.

The micro-CT results demonstrated an inverse relationship between implant volume and new bone formation. The solid nail design (TTC 1) occupied the largest implant volume (528.21 mm^3) but generated the least new bone formation (28.085 mm^3). In contrast, the 3D-printed lattice designs showed superior osteointegration potential. TTC 2, featuring the lowest implant volume (393.78 mm^3), achieved the highest new bone formation (145.37 mm^3). TTC 4, which incorporated both porous lattice and rib structures, showed a moderate implant volume (435.55 mm^3) while maintaining substantial new bone growth (137.81 mm^3). Notably, TTC 4 achieved the optimal balance between structural integrity and osteogenic capacity through its rib design. The bone growth distribution analysis revealed dense bone formation particularly in 3D-printed lattice areas, providing a favorable healing environment at the fusion sites. These findings highlight the advantages of lattice designs in orthopedic implants when optimized for both mechanical and biological requirements.

Advanced micro-CT scanning technology enables advanced bone growth assessment adjacent to metal implants while significantly reducing metal artifact interference. Using specialized software analysis, newly formed bone can be visualized in red and reconstructed into 3D images. This technology allows quantitative analysis of both the distribution pattern and volume of bone growth throughout the entire structure. This provides significant advantages over 2D histological section staining analysis, offering comprehensive evaluation of our implants' osteointegration properties.

Despite the occurrence of implant fractures in two pigs from the TTC 2 group, the bone growth induction effect of these porous designs remained remarkably significant. The TTC 2 group exhibited new bone volumes of 161.67 mm^3 and 108.85 mm^3 in the two subjects, these values substantially exceeded the average new bone volume observed in the TTC 1 group (28.85 mm^3), which featured a solid, smooth-surfaced nail design. This striking difference in bone formation, even in the presence of implant fractures, strongly suggests that the TTC 2 porous lattice structure significantly enhance the implant's capacity to promote bone adhesion and growth. These findings underscore the superior osteointegration

properties of textured, porous (lattice) surfaces compared to solid, smooth-surfaced implants, highlighting the potential of these designs to improve osseointegration in orthopedic applications, even in challenging conditions.

This study demonstrates significant strengths as the first pre-clinical animal study validation of a novel TTC nail design combining self-pressurizing leads with 3D-printed lattice structures, enabling comprehensive evaluation through mechanical testing and advanced micro-CT imaging analysis. This method enables quantitative assessment of bone formation patterns and volumes. The research provided clear comparisons between solid and lattice designs, offering practical insights for optimizing implant mechanical stability and biological integration. However, several limitations should be noted, including the small pig sample size, anatomical differences between pigs and humans affecting surgical approach, surgical complications including implant fractures, and the single 12-week evaluation timepoint. While these findings provide valuable guidance for future implant development, larger studies with longer follow-up periods would be beneficial to further validate these results.

Conclusion

The integration of 3D-printed diamond array lattice structures in TTC nail design showed that straightness, circularity, pitch distance and thread tip width were within the acceptable error, while the nail maintained cutting force and high compression efficiency. The mechanical strength test and micro-CT imaging results revealed both lattice structures and reinforcing ribs (TTC 4) provide an optimal balance between mechanical stability and biological integration, offering promising potential for improving tibiotalocalcaneal arthrodesis outcomes. This study concluded that titanium 3D printing technology can be applied for long intramedullary nail manufacturing with surface lattice design. However, reinforcing ribs are needed to provide enough mechanical strength.

Acknowledgements
N/A.

Author contributions
All authors reviewed the manuscript.

Funding
This manuscript was funded by Taiwan/project 112-2221-E-A49-009-MY3, 111-2327-B-A49-006 and 112-2327-B-A49 -002.

Data availability
No datasets were generated or analysed during the current study.

Declarations

Ethics approval and consent to participate
The in vivo pig study was reviewed and approved by the Taiwan Instrument Research Institute (Protocol No.: NLAC-112-M-041-R2). All procedures were conducted in compliance with the ARRIVE (Animal research: reporting of in vivo experiments) guidelines.

Consent for publication
Not applicable.

Further disclosure
N/A.

Competing interests
The authors declare no competing interests.

Received: 4 January 2025 / Accepted: 28 April 2025
Published online: 09 May 2025

References

1. Mendicino RW, Catanzariti AR, Saltrick KR, et al. Tibiotalocalcaneal arthrodesis with retrograde intramedullary nailing. J Foot Ankle Surg. 2004;43(2):82.
2. Jehan S, Shakeel M, Bing A, et al. The success of tibiotalocalcaneal arthrodesis with intramedullary nailing -A systematic review of the literature. Acta Orthop Belg. 2011;77:644.
3. Franceschi F, Franceschetti E, Torre G, et al. Tibiotalocalcaneal arthrodesis using an intramedullary nail: a systematic review. Knee Surg Sports Traumatol Arthrosc. 2016;24(4):1316.
4. Taylor J, Lucas DE, Riley A, et al. Tibiotalocalcaneal arthrodesis nails: A comparison of nails with and without internal compression. Foot Ankle Int. 2016;37(3):294.
5. Lu V, Tennyson M, Zhang J, Thahir A, et al. Ankle fusion with tibiotalocalcaneal retrograde nail for fragility ankle fractures: outcomes at a major trauma centre. Eur J Orthop Surg Traumatol. 2023;33(1):125.
6. Lu V, Tennyson M, Zhou A, et al. Retrograde tibiotalocalcaneal nailing for the treatment of acute ankle fractures in the elderly: a systematic review and meta-analysis. EFORT Open Rev. 2022;7(9):628.
7. Sundet M, Johnsen E, Eikvar KH, et al. Retrograde nailing, trabecular metal implant and use of bone marrow aspirate concentrate after failed ankle joint replacement. Foot Ankle Surg. 2021;27(2):123.
8. Donnenwerth MP, Roukis TS. Tibio-talo-calcaneal arthrodesis with retrograde compression intramedullary nail fixation for salvage of failed total ankle replacement: a systematic review. Clin Podiatr Med Surg. 2013;30(2):199.
9. Berkowitz MJ, Sanders RW, Walling AK. Salvage arthrodesis after failed ankle replacement: surgical decision making. Foot Ankle Clin. 2012;17(4):725.
10. Jehan S, Shakeel M, Bing AJ, et al. The success of tibiotalocalcaneal arthrodesis with intramedullary nailing–a systematic review of the literature. Acta Orthop Belg. 2011;77:644.
11. De Vries JG, Berlet GC, Hyer CF. Union rate of tibiotalocalcaneal nails with internal or external bone stimulation. Foot Ankle Int. 2012;33:11: 969.
12. Lee M, Choi WJ, Han SH, et al. Uncontrolled diabetes as a potential risk factor in tibiotalocalcaneal fusion using a retrograde intramedullary nail. Foot Ankle Surg. 2018;24(6):542.
13. Dujela M, Hyer CF, Berlet GC. Rate of subtalar joint arthrodesis after retrograde tibiotalocalcaneal arthrodesis with intramedullary nail fixation: evaluation of the RAIN database. Foot Ankle Spec. 2018;11(5):410.
14. Rammelt S, Pyrc J, Agren PH, et al. Tibiotalocalcaneal fusion using the hindfoot arthrodesis nail: a multicenter study. Foot Ankle Int. 2013;34(9):1245.
15. Levinson J, Reissig J, Schaheen e, et al. Complications and radiographic outcomes after tibiotalocalcaneal fusion with a retrograde intramedullary nail. Foot Ankle Spec. 2021;14(6):521.
16. Taniguchi N, Fujibayashi S, Takemoto M, et al. Effect of pore size on bone ingrowth into porous titanium implants fabricated by additive manufacturing: an in vivo experiment. Mater Sci Eng C Mater Biol Appl. 2016;59:690.
17. Hara D, Nakashima Y, Sato T, et al. Bone bonding strength of diamond-structured porous titanium-alloy implants manufactured using the electron beam-melting technique. Mater Sci Eng C Mater Biol Appl. 2016;59:1047.
18. Brown M, Cush G, Adams SB, et al. Use of 3D-Printed implants in complex foot and ankle reconstruction. J Orthop Trauma. 2024;38(4s):S17.

19. Pinzur MS, Schiff AP, Hamid K et al. Preliminary experience with commercially available trabecular metal tibial cones combined with a retrograde locked intramedullary nail for bony defects in tibiotalocalcaneal arthrodesis. Foot Ankle Spec 2024;19386400241236664.
20. Steele JR, Kadakia RJ, Cunningham DJ, et al. Comparison of 3D printed spherical implants versus femoral head allografts for tibiotalocalcaneal arthrodesis. J Foot Ankle Surg. 2020;59(6):1167.
21. Wong KW, Yang TH, Huang SF, et al. Biomechanical evaluation of a novel 3D printing tibiotalocalcaneus nail with trilobular cross-sectional design and self-compression effect. Comput Methods Programs Biomed Update. 2022;2:100072.
22. Abar B, Kwon N, Allen NB, et al. Outcomes of surgical reconstruction using custom 3D-Printed porous titanium implants for Critical-Sized bone defects of the foot and ankle. Foot Ankle Int. 2022;43(6):750.
23. Lin YS, Chang YZ, Yu JH, et al. Do dual-thread orthodontic mini-implants improve bone/tissue mechanical retention? Implant Dent. 2014;23(6):653.
24. Bhandari V. (2010) Design of machine elements; Tata McGraw-Hill Education.
25. Lord AE, Zhang L, Erickson JE, et al. Quantitative in vivo micro-computed tomography for monitoring disease activity and treatment response in a collagen-induced arthritis mouse model. Sci Rep. 2022;12:2863.
26. Arifvianto B, Leeflang MA, Zhou J, et al. Characterization of the porous structures of the green body and sintered biomedical titanium scaffolds with micro-computed tomography. Mater Charact. 2016;121:48.
27. Pyka G, Kerckhofs G, Schrooten J et al. The effect of Spatial micro-CT image resolution and surface complexity on the morphological 3D analysis of open porous structures. Mater Charact. 2013;87.

Publisher's note